Ionics (2010) 16:497–502
DOI 10.1007/s11581-010-0443-0

ORIGINAL PAPER

Effects of Sn doping on electrochemical characterizations of $Li[Ni_{1/3}Co_{1/3}Mn_{1/3}]O_2$ cathode material

Haibo Ren · Xiaoming Mu · Yanghui Huang · Zhongjing Li · Yunhong Wang · Ping Cai · Zhenghe Peng · Yunhong Zhou

Received: 4 September 2008 / Revised: 6 November 2008 / Accepted: 16 November 2008 / Published online: 23 May 2010

Abstract $Li[Ni_{1/3}Co_{1/3}Mn_{1/3}]O_2$ and Sn-doped $Li[Ni_{1/3}Co_{1/3}Mn_{1/3}]O_2$ cathode materials for lithium battery are synthesized by a solid-state method. The samples are characterized by X-ray diffraction, scanning electron microscope, electrochemical impedance spectroscopy (EIS), and charge–discharge test. The results show that the Sn-doped $Li[Ni_{1/3}Co_{1/3}Mn_{1/3}]O_2$ has a typical hexagonal α-$NaFeO_2$ structure and strawberry-like shape with uniform particle size. It has also been found that the Sn-doped $Li[Ni_{1/3}Co_{1/3}Mn_{1/3}]O_2$ reveals better electrochemical performances than that without Sn doping. The EIS results suggest that Sn presence decreases the total resistance of $Li[Ni_{1/3}Co_{1/3}Mn_{1/3}]O_2$, which should be related to the improvement on the electrochemical properties.

Keywords Li-ion batteries · Cathodes · Electrochemical characterizations · Charging/discharging · XRD

H. Ren
Department of Chemistry and Chemical Engineering,
Henan University of Urban Construction,
Pingdingshan 467044, People's Republic of China

H. Ren · Y. Huang · Z. Li · Y. Wang · P. Cai · Z. Peng (✉) · Y. Zhou
Department of Chemistry, Wuhan University,
Wuhan 430072 Hubei, China
e-mail: pengzh@chem.whu.edu.cn

X. Mu
Environment and Chemistry College,
Luoyang Institute of Science and Technology,
Luoyang 471023 Henan, China

Introduction

Lithium cobalt oxide ($LiCoO_2$), as a cathode material for lithium secondary battery, has widely been used in various fields, but it has some drawbacks such as the high cost of cobalt, toxicity, and instability [1, 2]. Therefore, many researchers have been extensively studying alternatives to $LiCoO_2$. Among all of the candidates, $Li[Ni_{1/3}Co_{1/3}Mn_{1/3}]O_2$ is proposed as a promising material to replace $LiCoO_2$ [3–6] due to its higher reversible capacity, good cycling performance, and structural stability. However, the lower the tap density of these layered compounds, the poorer is the rate capability. The capacity fading of long-term cycling [3, 7–10] is also the main obstacle when applied as cathode materials in lithium ion batteries. To further improve performances of $Li[Ni_{1/3}Co_{1/3}Mn_{1/3}]O_2$, small amounts of additional dopants like Mg, Mo, Cr, Al, and Fe into the Li $[Ni_{1/3}Co_{1/3}Mn_{1/3}]O_2$ lattice have been reported [11–14], which suggested that cationic substitution for transition metals appeared to be a good method to modify the structural and electrochemical properties of the $Li[Ni_{1/3}Co_{1/3}Mn_{1/3}]O_2$. Tin was also used as dopant to modify the electrode materials [15–18]. However, to our knowledge, it has not been applied to optimize the $Li[Ni_{1/3}Co_{1/3}Mn_{1/3}]O_2$. In this paper, we would like to introduce the effect of Sn doping on the morphology of $Li[Ni_{1/3}Co_{1/3}Mn_{1/3}]O_2$, and the electrochemical properties of Sn-doped $Li[Ni_{1/3}Co_{1/3}Mn_{1/3}]O_2$ will also be discussed in detail.

Experimental

Powders of $Li[Ni_{1/3}Co_{1/3}Mn_{1/3}]O_2$ and Sn-doped $Li[Ni_{1/3}Co_{1/3}Mn_{1/3}]O_2$ were prepared by the solid-state method. $LiOH{\cdot}H_2O$, $Ni(OH)_2$, Co_2O_3, Mn_3O_4, and SnO_2

were used as the starting materials in a stoichiometric Li $[Ni_{1/3}Co_{1/3}Mn_{1/3}]_{1-x}Sn_xO_2$ (x=0, 0.01). These reagents were mixed, thoroughly ground with the help of the appropriate amount of alcohol. It is important to add alcohol to the mixture, not only to facilitate mixing and grinding but also to be used as "fuel" to ensure the homogeneity during the calcinations. The ground mixture was calcined at 850 °C for 20 h in air to yield products.

X-ray diffraction (XRD) measurements of the $Li[Ni_{1/3}Co_{1/3}Mn_{1/3}]_{1-x}Sn_xO_2$ materials were carried out using XRD (Shimadzu XRD-6000) with Cu $K\alpha$ radiation (λ=1.54056 Å). Lattice parameters and unit cell volumes were calculated by a least squares method with FullProf Suite program. Particle morphology of the powders after calcinations was observed using a scanning electron microscope (SEM, QUANTA-200, Holland). The specific areas of the $Li[Ni_{1/3}Co_{1/3}Mn_{1/3}]_{1-x}Sn_xO_2$ samples were deduced from nitrogen adsorption experiments (BET method). X-ray photoelectron spectra (XPS) are recorded by a Kratos Model XSAM 800 spectrometer equipped with an Mg-Kα X-ray source (hν=1,253.6). Electrochemical impedance measurements were carried out using an Electrochemical System (Reference 600, USA) in the frequency range of 10 mHz to10^5 Hz with an excitation signal of 5 mV.

Electrochemical charge–discharge experiments were performed by assembling model test cells. Test cathode electrodes were prepared by mix 80:15:5 (mass ratio) of active material, acetylene black, and PTFE binder, respectively, in isopropyl alcohol. The model test cells were assembled with the electrode prepared above as cathode, lithium metal as anode, and Celgard 2300 film as separator in an argon-filled glove box. The electrolyte was 1 M $LiClO_4$ dissolved in EC+DMC (1:1 volume ratio).

All tests were performed at room temperature.

Results and discussion

Figure 1 shows XRD patterns of the $Li[Ni_{1/3}Co_{1/3}Mn_{1/3}]_{1-x}Sn_xO_2$ (x=0, 0.01). All peaks are sharp and well-defined, suggesting that compounds are generally well crystallized, which can be indexed to the hexagonal α-$NaFeO_2$ structure (space group, $R\bar{3}m$). Especially, no impurity peaks of Li_2SnO_3 were observed for x=0.01, indicating that phase-pure $Li[Ni_{1/3}Co_{1/3}Mn_{1/3}]_{0.99}Sn_{0.01}O_2$ with a layered structure can be obtained [16]. The peak splits of (006)/(102) and (108)/(110) doublets mean the formation of a highly hexagonal ordered layer structure [9, 19]. For the $I_{(003)}/I_{(104)}$ ratios of the undoped and the doped $Li[Ni_{1/3}Co_{1/3}Mn_{1/3}]O_2$, 1.39 and 1.58, respectively, which are more than 1.2, no undesirable cation mixing takes place [20]. Moreover, Sn-doped $Li[Ni_{1/3}Co_{1/3}Mn_{1/3}]O_2$ holds more

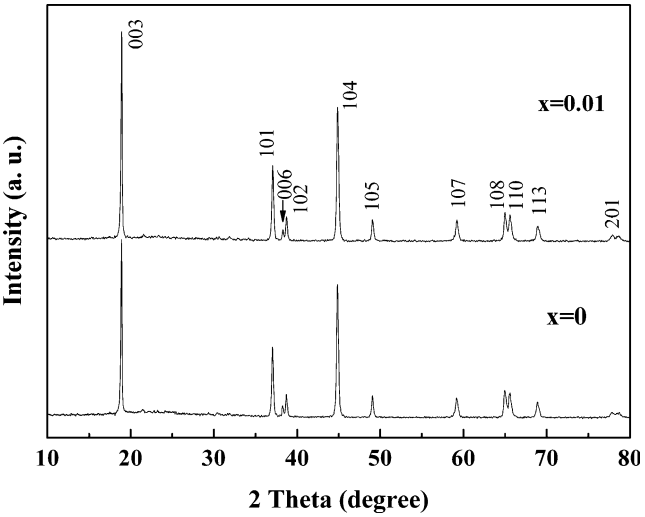

Fig. 1 X-ray diffraction patterns of the $Li[Ni_{1/3}Co_{1/3}Mn_{1/3}]_{1-x}Sn_xO_2$ (x=0, 0.01)

excellent structural integrity (bigger $I_{(003)}/I_{(104)}$), i.e., lower cation mixing, which indicates that a small amount of Sn substitution for transition metals could prevent the occupancy of the Li^+ layers by the transition metal ions. In addition, the lattice parameters of the undoped $Li[Ni_{1/3}Co_{1/3}Mn_{1/3}]O_2$ are a=2.8612 Å, c=14.2202 Å, and V=100.8138 $Å^3$, and those of the doped $Li[Ni_{1/3}Co_{1/3}Mn_{1/3}]O_2$ are a=2.8761 Å, c=14.3266 Å, and V=102.6287 $Å^3$. Clearly, the parameters of the latter are larger than those of the undoped $Li[Ni_{1/3}Co_{1/3}Mn_{1/3}]O_2$, which should be the result that Sn^{4+} ions occupy partly the transition metal sites. If an Sn^{4+} (0.71 Å) occupies an Li^+ (0.68 Å) site which causes to form an $Sn_{Li}^{\cdot\cdot\cdot}$ defect and three lithium vacancies, V_{Li}', the cell volume would decrease. Therefore, we believe that it is the Sn^{4+} ions occupying the Ni^{2+} (0.69 Å), Co^{3+} (0.62 Å), or Mn^{4+} (0.60 Å) ions sites that make the lattice parameters increase. To keep the electric charge in equilibrium, part Co^{2+} ions are not oxidized to form $Co(II)_{Co}{}'$ defects, which can release a free electron into conduction band to increase the electronic conductivity. The ionization reaction formula of $Co(II)_{Co}{}'$ defect is as follows: $Co(II)_{Co}{}' \rightarrow Co + e'$. Volume expansion of the unit cell assists the intercalation and deintercalation of the Li^+ ions during electrochemical processes, which would decrease the impedance and increase the conductivity.

Figure 2 shows the measured XPS spectrum of Sn 3d measured for $Li[Ni_{1/3}Co_{1/3}Mn_{1/3}]_{0.99}Sn_{0.01}O_2$. The signal could be identified as Sn^{+4} by using reference measurement of pure SnO_2 and handbook of the XPS [21].

SEM images of the two samples of $Li[Ni_{1/3}Co_{1/3}Mn_{1/3}]O_2$ and $Li[Ni_{1/3}Co_{1/3}Mn_{1/3}]_{0.99}Sn_{0.01}O_2$ are illustrated in Fig. 3. The powder of the undoped one consists of grains with irregular shape, and some of the particles are aggregated (Fig. 3, a). However, the morphology of the

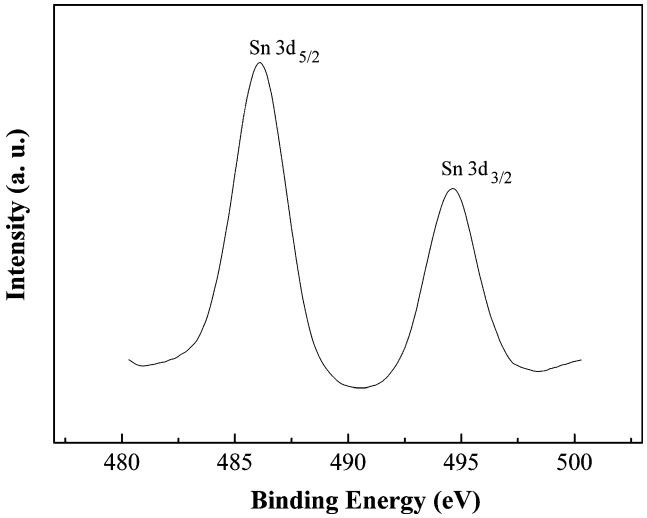

Fig. 2 X-ray photoelectron spectrum of Sn 3d measured for $Li[Ni_{1/3}Co_{1/3}Mn_{1/3}]_{0.99}Sn_{0.01}O_2$

Sn-doped one is obviously different from the undoped one. From Fig. 3, b1, the powder of the Sn-doped one is composed of dispersed spherical grains. It is clear that the Sn doping makes the particle size smaller and more uniform. The smaller particles tend to improve the capacity of the battery by reducing the ion diffusion pathway during insertion and desertion processes of Li^+ ion [22]. The uniform particle size distribution leads to the uniform depth of charge of each particle, which increases the utilization of the material to enhance the overall battery performance.

Interestingly, detailed observation of the Sn-doped $Li[Ni_{1/3}Co_{1/3}Mn_{1/3}]O_2$ particles in bigger multiples (Fig. 3, b2 and b3) shows that the particles are composed of strawberry-shaped spheres, whose surface exists a great deal of granules. Moreover, we can find from the sphere marked with an arrow in Fig. 3, b3, that these strawberry-shaped spheres are not formed through agglomeration of those granules, which are just outgrowths on the spheres. It is strongly advised that the special morphology should be due to Sn doping, which possibly results in the difference in surface energy and provides the seeds of the strawberries. Undoubtedly, the surface area of the Sn-doped $Li[Ni_{1/3}Co_{1/3}Mn_{1/3}]O_2$ particles with strawberry-shaped spheres is increased relative to the particles with glazed faces. By testing with BET method, the specific surface area of the Sn-doped $Li[Ni_{1/3}Co_{1/3}Mn_{1/3}]O_2$ particles, 2.556 m^2g^{-1}, is obviously bigger than that of the undoped $Li[Ni_{1/3}Co_{1/3}Mn_{1/3}]O_2$, 1.681 m^2g^{-1}.

As is well known, the influence of particle size, morphology, and surface area to the battery performance is of great importance. We believe that differences of both compounds in size, morphology, and surface area should result in differences in their electrochemical performance.

Rate capability is one of the important electrochemical characteristics of a lithium secondary battery required for power storage application. In the present study, rate

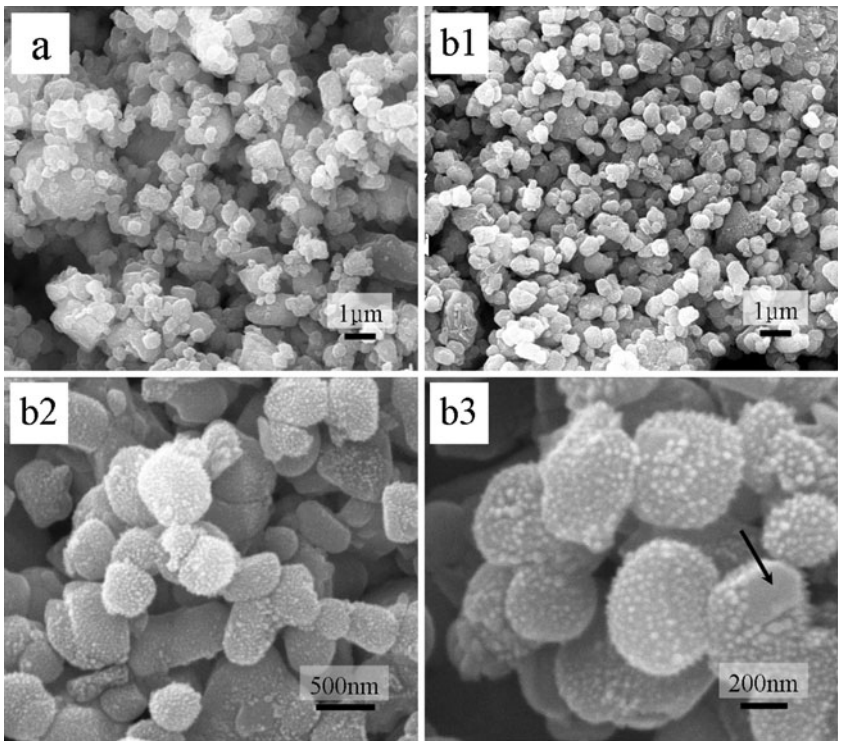

Fig. 3 Scanning electron microscope images of the undoped $Li[Ni_{1/3}Co_{1/3}Mn_{1/3}]O_2$ (*a*) and the Sn-doped $Li[Ni_{1/3}Co_{1/3}Mn_{1/3}]O_2$ (*b1–b3*)

capabilities are investigated, respectively, at the constant current of 20 and 200 mAg^{-1} between 3 and 4.3 V at room temperature. According to Fig. 4a, b, the initial discharge capacity of both compounds decreases by increasing the discharge current. The Sn-doped $Li[Ni_{1/3}Co_{1/3}Mn_{1/3}]O_2$ delivers the discharge capacities of 168 and 165 $mAhg^{-1}$ (coulombic efficiency, 87% and 91%) at 20 and 200 mAg^{-1}, respectively, while the undoped sample with discharge capacities of 156 and 152 $mAhg^{-1}$ (coulombic efficiency, 85% and 88%). Obviously, the rate capability and capacity of the Sn-doped $Li[Ni_{1/3}Co_{1/3}Mn_{1/3}]O_2$ is increased in comparison with the undoped one. As mentioned previously, it is probably caused by Sn doping which lowers the electrochemical impedance and increases the conductivity. In addition, from the perspective of particle morphology, it should also be ascribed to the Sn-doped sample holding smaller particle size and larger specific surface.

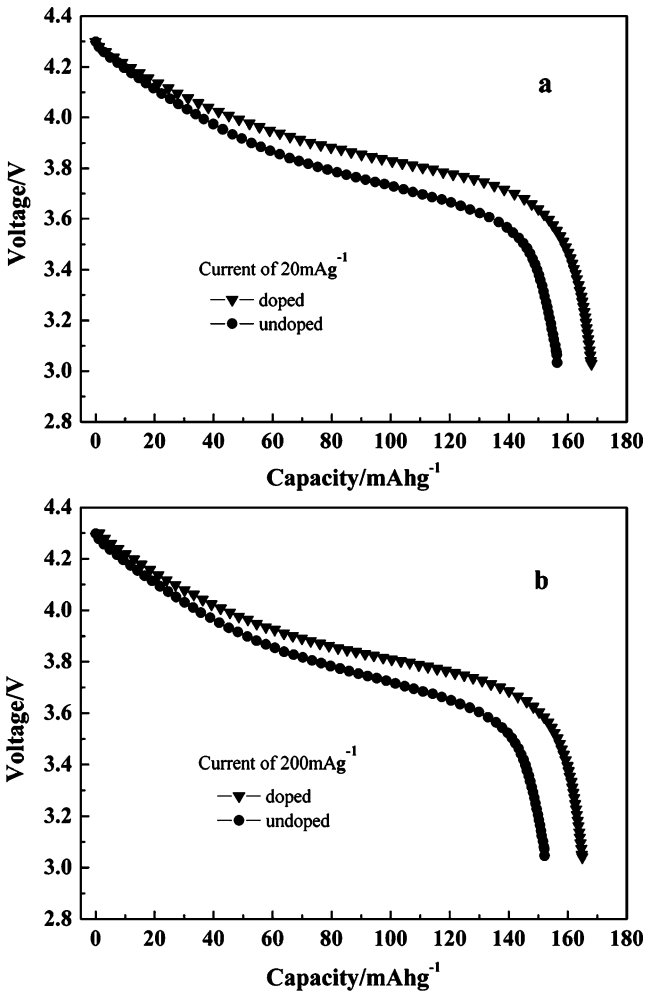

Fig. 4 Initial discharge curves for the undoped $Li[Ni_{1/3}Co_{1/3}Mn_{1/3}]O_2$ and the Sn-doped $Li[Ni_{1/3}Co_{1/3}Mn_{1/3}]O_2$ operated in the voltages range of 3~4.3 V at different current densities: (**a**) 20 and (**b**) 200 mAg^{-1}

It is noticeable that the discharge curves of the undoped sample are below those of the Sn-doped one, whether at a current density of 20 or 200 mAg^{-1}. This means that the electrode composed of the undoped sample shows a higher polarization than that of the Sn-doped sample, indicating that the Sn doping reduces the polarization of the cathode/electrolyte interface in the cell. The reduction of the cell polarization may be ascribed to the decrease in cell resistance with respect to specific surface area because the Sn-doped sample has larger specific surface area, which leads to the better electrochemical performance of the Sn-doped sample due to the improvement in electronic conductivity of the compound [23].

In order to monitor cyclic performance of the two samples, broader voltage and higher current density, the voltage range 2.5~4.6 V with a current density of 200 mAg^{-1} was adopted. Here, 4.6 V is chosen as the upper limit because the critical upper limit of $LiNiO_2$ and $LiCoO_2$ is 4.6 V [24, 25]. As we know, when an electrode is working under bigger currents, a lot of Li^+ should be intercalated or deintercalated from electrode material at a higher speed, which demands the electrode material to have enough Li^+ used and hold better layer structure to ease the movement of Li^+. If an electrode is employed under higher voltages, the higher capacity can be gained, but the decomposition of the electrolyte at the surface of electrode material will get more serious, which brings the rapid decay of the cell capacity along with charge–discharge cycles. Therefore, it would be a severe test for the structure and performance of electrode materials if the electrodes are engaged in rigorous conditions of bigger currents and higher voltages. Figure 5 shows the cycling performance of the Sn-doped and undoped samples under given conditions.

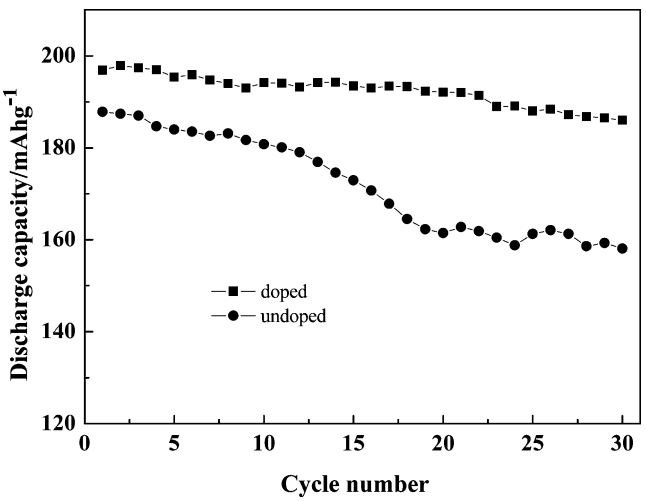

Fig. 5 Specific discharge capacity as a function of cycle number for two samples operated in the voltage range of 2.5~4.6 V at a current density of 200 mAg^{-1}

Table 1 The charge–discharge data for two samples in the voltage range of 2.5~4.6 V at a current density of 200 mAg^{-1}

Samples	First cycle Q_{charge} ($mAhg^{-1}$)	First cycle $Q_{discharge}$ ($mAhg^{-1}$)	30th cycle $Q_{discharge}$ ($mAhg^{-1}$)	Capacity retention (%)
The doped	229	197	185	94
The undoped	221	188	158	84

Table 1 also gives charge–discharge capacities and capacity retention rations of the two samples under the same conditions. Obviously, even though the Sn-doped material is working under rigorous conditions, the initial discharge capacity of 197 $mAhg^{-1}$ can be achieved and still present better cycling performance, retaining the discharge capacity 185 $mAhg^{-1}$ at the end of the 30th cycle. By comparison, the undoped material displays worse electrochemical performances. The initial discharge capacity is 188 $mAhg^{-1}$ and only 158 $mAhg^{-1}$ at the end of the 30th cycle. So the Sn doping assuredly enhance the structural integrity of Li $[Ni_{1/3}Co_{1/3}Mn_{1/3}]O_2$ and depress reaction activity of surface with the electrolyte.

Electrochemical impedance measurements were carried out to provide more information for the improved electrochemical property. Figure 6 shows the impedance spectra of $Li[Ni_{1/3}Co_{1/3}Mn_{1/3}]O_2$ and the $Li[Ni_{1/3}Co_{1/3}Mn_{1/3}]_{0.99}Sn_{0.01}O_2$ electrodes at pristine state and charged to 4.3 V. A semicircle is observed in the high frequency domain for both samples at the pristine state (Fig. 6a), and its origin has been ascribed to the lithium ion migration through the interface between the surface layer of the particles and the electrolyte [26, 27]. The calculated resistance of the pristine $Li[Ni_{1/3}Co_{1/3}Mn_{1/3}]O_2$ electrode is about 23 Ω. For the $Li[Ni_{1/3}Co_{1/3}Mn_{1/3}]_{0.99}Sn_{0.01}O_2$ electrode, this resistance is about 19 Ω, lower than that of the $Li[Ni_{1/3}Co_{1/3}Mn_{1/3}]O_2$ electrode. When the electrodes are charged to 4.3 V (Fig. 6b), no significant change is observed in this semicircle. However, a new semicircle appears in the relatively low frequency region, whose origin may be assigned to the charge transfer resistance (R_{ct}). As shown in Fig. 6b, the $Li[Ni_{1/3}Co_{1/3}Mn_{1/3}]O_2$ electrode has a higher R_{ct} than that of the $Li[Ni_{1/3}Co_{1/3}Mn_{1/3}]_{0.99}Sn_{0.01}O_2$ electrode. Hence, the $Li[Ni_{1/3}Co_{1/3}Mn_{1/3}]_{0.99}Sn_{0.01}O_2$ electrode shows lower total resistance (sum of surface layer resistance and charge transfer resistance). Electrochemical impedance is a major part of internal resistance of a battery, and small impedance is favorable for the insertion and deinsertion of lithium ions during the charge and discharge process. According to the electrochemical impedance spectroscopy analysis above, we can conclude that the $Li[Ni_{1/3}Co_{1/3}Mn_{1/3}]O_2$ material becomes more conductive with Sn doping and displays the improved electrochemical properties, which corresponds with the parts discussed above.

Conclusions

Our experimental results reveal that the addition of Sn has an important effect on the physical and electrochemical performance of $Li[Ni_{1/3}Co_{1/3}Mn_{1/3}]O_2$. It changes the morphologies of particles and uniforms the sizes of grains. It increases the structural integrity and decreases the total resistance during cycling. It improves the capacity, rate

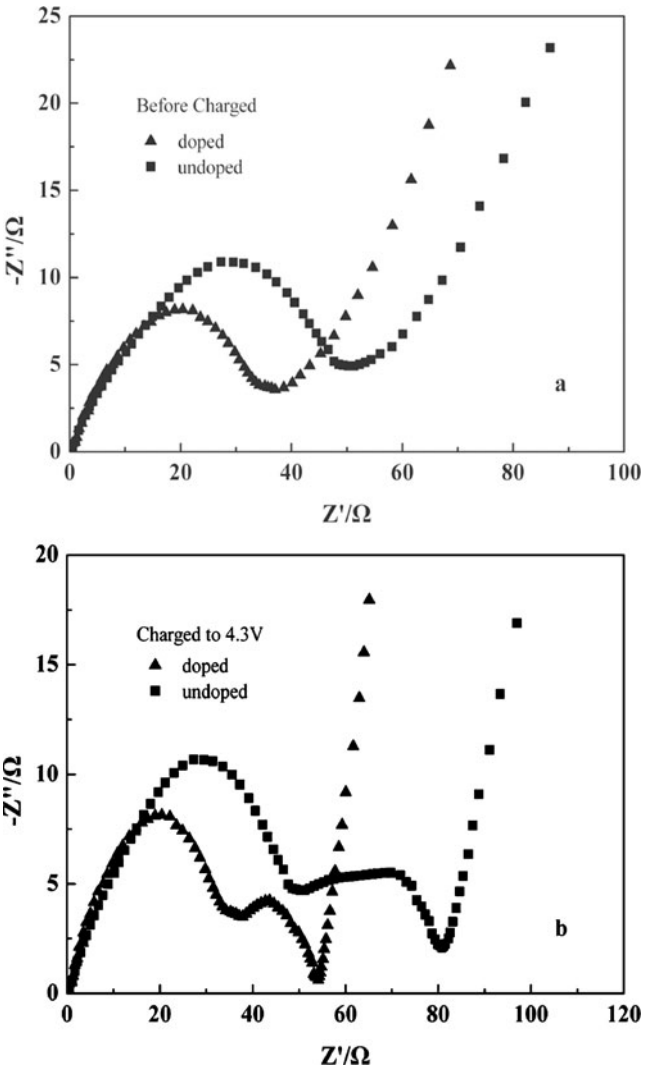

Fig. 6 The impedance spectra of the undoped and the Sn-doped Li $[Ni_{1/3}Co_{1/3}Mn_{1/3}]O_2$ electrodes at different electrochemical states

capability, and cyclability. Hereby, the Sn doping on $Li[Ni_{1/3}Co_{1/3}Mn_{1/3}]O_2$ is an effective approach to obtain a promising alternative cathode material for lithium battery.

Acknowledgements We gratefully acknowledge the financial support from the National Nature Science Foundation of China (No. 29833090, No. 29771025, and No. 20573078).

References

1. Menetrier M, Saadoune I, Levasseur S, Delmas C (1999) J Mater Chem 9:1135
2. Ohzuku T, Makimura Y (2001) Chem Lett 8:744
3. Shaju KM, Subba Rao GV, Chowdari BVR (2002) Electrochim Acta 48:145
4. Shin YJ, Choi WJ, Hong YS, Yoon S, Ryu KS, Chang SH (2006) Solid State Ion 177:515
5. Li D, Muta T, Zhang L, Yoshio M, Noguchi H (2004) J Power Sources 132:150
6. Reddy MV, Subba Rao GV, Chowdari BVR (2006) J Power Sources 159:263
7. Song MY, Lee R (2002) J Power Sources 111:97
8. Lee MH, Kang YJ, Myung ST, Sun YK (2004) Electrochim Acta 50:939
9. Cho TH, Park SM, Yoshio M, Hirai T, Hideshima Y (2005) J Power Sources 142:306
10. Yoon WS, Grey CP, Balasubramanian M, Yang XQ, McBreen J (2003) Chem Mater 15:3161
11. Kim GH, Myung ST, Kim HS, Sun YK (2006) Electrochim Acta 51:2447
12. Park SH, Oh SW, Sun YK (2005) J Power Sources 146:622
13. Suna Y, Xia Y, Noguchi H (2006) J Power Sources 159:1377
14. Liu DT, Wang ZX, Chen LQ (2006) Electrochim Acta 51:4199
15. Aroutiounian VM, Arakelyan VM, Shahnazaryan GE, Hovhannisyan HR, Wang H, John A (2007) Sol Energy 81:1369
16. Li JG, He XM, Zhao RS, Wan CR, Jiang CY, Xia DG, Zhang SC (2006) J Power Sources 158:524
17. Jayaprakash N, Kalaiselve N (2007) Electrochem Commun 9:620
18. Ma XL, Wang CW, Cheng JG, Sun JT (2007) Solid State Ionics 178:125
19. Rougier A, Gravereau P, Delmas C (1996) J Electrochem Soc 143 (4):1168
20. Hwang BJ, Santhanam R, Chen CH (2003) J Power Sources 114:244
21. Moulder JF, Stickle WF, Sobol PE (1992) Handbook of X-ray photoelectron spectroscopy
22. Cho J, Park B (2001) J Power Sources 92:35
23. Gabrisch H, Wilcox JD, Doeff MM (2006) Electrochem Solid State Lett 9:A360
24. Ohzuku T, Makimura Y (2001) Chem Lett 7:642
25. Paulsen JM, Thomas CL, Dahn JR (2000) J Electrochem Soc 147:861
26. Aurbach D, Levi M, Levi E, Teller H, Markovsky B, Salitra G, Heider U, Heider L (1998) J Electrochem Soc 145:3024
27. Levi M, Salitra G, Markovsky B, Teller H, Aurbach D, Heider U, Heider L (1999) J Electrochem Soc 146:12